TRANSLATIONAL CHEMISTRY
AN INTERFACE JOURNAL
HTTPS://WWW.TRANSLATIONALCHEMISTRY.COM/

ORIGINAL ARTICLE | DOI: 10.5584/translationalchemistry.v1i2.250

Fluorous Tails and Anion Effects as Dual Drivers of Ionic Self-Assembly in Triazolium Ionic Liquid Crystals

Ignazio Fiduccia[1,¥], Carla Rizzo[1,¥], Davide Ricci[1], Andrea Pace[1], Ivana Pibiri[*]

[1]Department of Biological, Chemical and Pharmaceutical Sciences and Technologies (STEBICEF), University of Palermo, Viale delle Scienze, Ed. 17, 90128 Palermo, Italy. [¥]Both authors contributed equally to this work.

Received: 10 December 2025 **Accepted:** 17 December 2025 **Available Online**: 24 December 2025

Abstract

A series of perfluoroheptyl-substituted 1,2,4-triazolium ionic liquid crystals differing for the phenyl alkoxy substitution pattern (4-substituted, 3,4-substituted, 3,5-substituted) and the counter-ion (OTf^-, PF_6^-, NTf_2^-) have been investigated. Anion-exchange metathesis of three triazolium triflates gave five additional salts, all characterized by Differential Scanning Calorimetry and Polarized Optical Microscopy. Data reveal a consistent counter-ion effect: NTf_2^- derivatives exhibit lower melting and clearing temperatures than their PF_6^- analogues. Mesophase breadth and complexity are primarily dictated by cation structure, with 3,5-disubstituted derivatives showing narrow mesophase windows, while 4- and 3,4-substituted cations exhibit broader ranges and multiple transitions. Polarized Optical Microscopy observations corroborate smectic behavior in single-chain derivatives and layered or columnar organization in dialkyloxy analogues. Besides, dendritic growth in the 3,4-substituted PF_6^- salt suggests discotic aggregation. Overall, the combined effects of selective anion exchange and controlled peripheral substitution provide an effective strategy to tune mesophase type, thermal behavior and supramolecular organization in perfluoroalkyl triazolium ionic liquid crystals, offering transferable design principles for engineering fluorinated ILCs with targeted properties for structured electrolytes, ion-conductive materials and responsive soft devices.

Keywords: Fluorinated materials, Ionic liquid crystals, Anion methatesis, Heterocyclic compounds , Triazolium salts.

1. Introduction

Ionic liquid crystals (ILCs) are low-melting organic salts that combine persistent orientational order with ionic mobility, so they occupy an intermediate regime between conventional liquid crystals and ionic liquids [1–3]. The coexistence of anisotropic supramolecular order and mobile charge carriers gives rise to combined properties such as low volatility, ionic conductivity and directional supramolecular order, which make ILCs attractive for applications in energy storage, electrochemical devices, sensing and separation technologies [4–7]. Early work on ILCs focused on classical cation families such as imidazolium and pyridinium thanks to their synthetic accessibility and well-studied self-assembly behavior [1,2]. In recent years the field has broadened to include alternative heterocyclic scaffolds, including oxadiazole and triazole cores, which offer distinct electronic distributions and substitution patterns and therefore additional handles to tune molecular shape and mesophase formation [8–12]. Synthetic approaches that transform 1,2,4-oxadiazoles into 1,2,4-triazoles by ANRORC mechanism (Addition of Nucleophiles, Ring Opening and Ring Closure) have been widely used to introduce perfluoroalkyl substituents on the heterocyclic core in a concise and reliable manner [8,13,14]. Incorporation of perfluoroalkyl segments into mesogenic molecules modifies nanoscale segregation and molecular packing relative to purely hydrocarbon analogues. Fluorous domains often stabilize smectic or columnar arrangements while affecting thermal stability and ionic transport [5,9,15]. This triphilic architecture, in which ionic, hydrocarbon and fluorous subdomains coexist, leads to distinctive mesoscale organization and to opportunities for designing directional ionic channels and selective supramolecular assemblies [16–18]. The specific balance between van der Waals interactions among alkyl chains, fluorous segregation and Coulombic forces determines whether a system favors smectic layering, columnar stacking or other mesomorphic symmetries [19,16,20]. Counter-ion identity represents a second, experimentally accessible design variable that strongly affects phase behavior [1,11,21]. Anion size, polarizability and charge delocalization influence ion pairing, lattice cohesion

***Corresponding author:** Ivana Pibiri | ivana.pibiri@unipa.it

and the free volume available for chain motion. Systematic anion exchange by metathesis is therefore a routine and effective strategy to probe how the anion controls melting and clearing temperatures, mesophase breadth and ionic dynamics [11,21]. Within the 1,2,4-triazolium family, previous studies have shown that perfluoroalkyl tail length, the number and position of alkoxy substituents on the aromatic ring, and the identity of the counter-ion collectively govern mesophase type, including smectic, columnar or other mesophase types, and the thermal stability of those phases [5,10,11,18]. Because these structural and ionic variables are interdependent, comparative studies that hold the perfluoroalkyl tail constant while varying only peripheral alkoxy substitution and counter-ion provide a direct route to separate geometric and ionic effects on mesomorphism. Such systematic datasets are valuable both for mechanistic interpretation and for practical design rules. To facilitate direct comparison with earlier studies, **Scheme 1** collects selected literature triazolium salts together with the new compounds prepared in this work. The upper panel reproduces the 4-substituted triazolium triflates and the related NTf_2^- analogue described by Rizzo *et al.* [21] and the 3,5-disubstituted triazolium triflate reported by Riccobono *et al.* [11]. The lower panel presents the triazolium salts synthesized in the present study, which differ from previous ones in the pattern of alkoxy substitution, on the phenyl ring and in the counter-ion. Specifically, a series of dialkyloxy-phenyl 1,2,4-triazolium salts bearing a fixed perfluoroheptyl substituent has been synthesized. The cationic cores share the same perfluoroalkyl tail but differ in the position of the long alkoxy chains on the phenyl ring, which were introduced in the 4-, 3,4- and 3,5-arrangements. Selected triazolium triflates were converted into PF_6^- and NTf_2^- salts by controlled anion metathesis. The products were characterized by differential scanning calorimetry (DSC) and polarized optical microscopy (POM). Because the perfluoroalkyl tail is constant across the series, this dataset allows us to isolate the separate contributions of peripheral substitution pattern and counter-ion identity on mesophase type, transition temperatures and mesoscale ordering in this family of perfluoroalkyl triazolium ILCs. This study complements and extends recent triazolium ILC work in the literature and provides a systematic dataset to isolate the roles of peripheral substitution and anion identity.

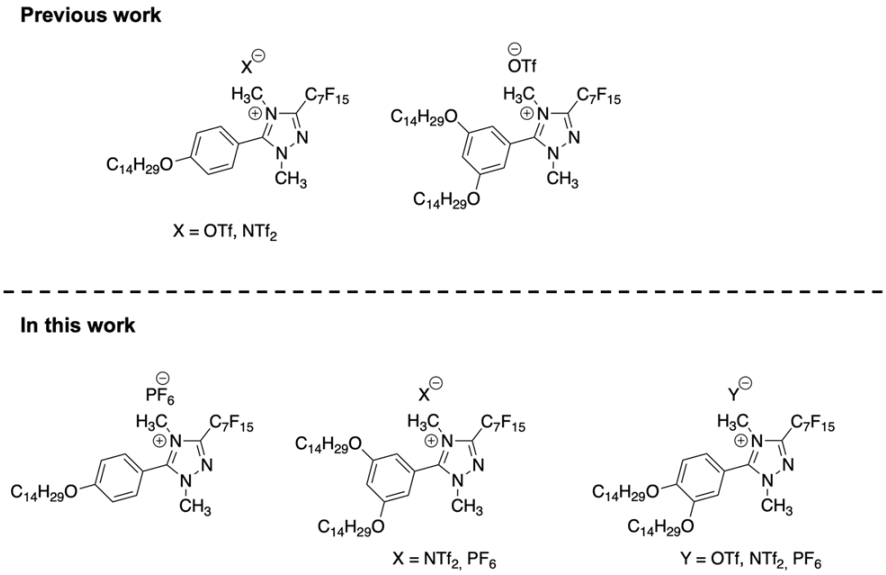

Scheme 1 | Structures of triazolium salts. Upper panel: literature triazolium salts reproduced for comparison; 4-substituted triazolium triflates and the corresponding NTf_2^- derivative from Rizzo *et al.* [21], and the 3,5-disubstituted triazolium triflate from Riccobono *et al.* [11]. Lower panel: triazolium salts synthesized in this work.

2. Materials and methods

2.1. General

2.1.1. Materials

Piperonal, sodium hydroxide, hydroxylamine hydrochloride, methylhydrazine, boron tribromide, pentadecafluorooctanoyl chloride, potassium carbonate, 1-bromotetradecane, methyl trifluoromethanesulfonate, ethyl acetate, petroleum ether, dimethyl sulfoxide, *N,N*-dimethylformamide, toluene, chloroform, methanol, ethanol (96%), acetonitrile, and pyridine were purchased from a commercial source and used as received. Two triazolium triflates (*5-(3,5-bis(tetradecyloxy)phenyl)-1,4-dimethyl-3-(perfluoroheptyl)-1H-1,2,4-triazol-4-ium trifluoromethanesulfonate* and *5-(4-(tetradecyloxy)phenyl)-1,4-dimethyl-3-(perfluoroheptyl)-1H-1,2,4-triazol-4-ium trifluoromethanesulfonate*) were synthesized as described by Rizzo *et al.* [21] and Riccobono *et al.* [11].

2.1.2. Methods

^{1}H-NMR spectra were recorded on Bruker instrument operating at 300 MHz MHz spectrometer. Chemical shifts were referenced to the residual solvent peak. High-resolution mass analyses (HPLC/ESI/Q-TOF HRMS) were performed using HPLC/MS-grade water and acetonitrile containing 0.1% (v/v) formic acid. Chromatographic separations were carried out on an Agilent 1260 Infinity system equipped with a Luna Omega Polar C18 column (5 μm, 150 x 2.1 mm) and a Phenomenex C18 guard cartridge (4 x 3 mm). The flow rate was set at 1 mL/min whilst the column

maintained at 40 °C. A linear gradient was employed as follows: 95% to 5% water over 10 min, 5% to 95% water over the next 10 min, and finally 95% to 5% water during the last 5 min. Sample injections were 10 µL, and chromatograms were monitored using MS TIC. Mass spectra were registered on an Agilent 6540 UHD accurate-mass Q-TOF spectrometer equipped with a Dual AJS ESI source working in positive mode. N_2 was used as a desolvation gas at 300 °C and a flow rate of 9 L/min. The nebulizer pressure was set to 45 psi. The Sheath gas temperature was set at 350 °C and a flow of 12 L/min. The capillary voltage was adjusted to 3.5 kV, and the fragmentor to 110 V. Data were collected over an m/z range of 150-2000. POM was conducted using a Zeiss Axio Imager.A2m microscope (Carl Zeiss, Göttingen, Germany) equipped with a Linkham LTS420E hot stage controlled by a Linkpad T95-LTS unit. Samples were mounted between a glass slide and coverslip and subjected to heating and cooling cycles at 5 °C·min^{-1}. Photomicrographs were captured with an Axiocam ICC1 camera at magnifications of 5x, 10x, and 20x under cross-polarized illumination. DSC was performed using a TA Instruments 2920 DSC system equipped with a refrigerated cooling accessory. Approximately 4 mg of sample were sealed in aluminum TA Tzero Hermetic Pans. Heating and cooling scans were conducted at 10 ° C·min^{-1} under a nitrogen flow of 60 mL·min-1. Each analysis consisted of three consecutive heating and cooling cycles in a range comprised between -50 °C and 220 °C in dependence of compound analyzed.

2.2. Synthesis of 3,4-Methylenedioxybenzonitrile (1)

Piperonal (6.1 g; 40.6 mmol) was dissolved in DMSO. $NH_2OH{\cdot}HCl$ (5.2 g; 1.9 mol eq.) was added, and the mixture was stirred at room temperature for 10 min. The DMSO was then removed by sublimation using a freeze dryer. The crude residue was isolated and purified by column chromatography, using a 10:1 petroleum ether/ethyl acetate mixture as the eluent. A white solid was obtained. **3,4-Methylenedioxybenzonitrile (1)**: white solid. Yield = 82%. ^{1}H NMR (300 MHz, $CDCl_3$) δ: 7.21 (dd, J = 8.1, 1.5 Hz, 1H), 7.04 (d, J = 1.5 Hz, 1H), 6.86 (d, J = 8.1 Hz, 1H), 6.07 (s, 2H).

2.3. Synthesis of N-Hydroxy-1,3-benzodioxole-5-carboximidamide (2)

3,4-Methylenedioxybenzonitrile (4.9 g; 33.3 mmol) was dissolved in EtOH (70 mL), and a mixture of two aqueous solutions of NaOH (1.6 g; 1.2 mol eq.) and $NH_2OH{\cdot}HCl$ (2.7 g; 1.2 mol eq.) was added. The reaction mixture was refluxed for 6 h. After evaporation to dryness, water was added to the residue, leading to the precipitation of the N-Hydroxy-1,3-benzodioxole-5-carboximidamide (2). A white solid was obtained. **N-Hydroxy-1,3-benzodioxole-5-carboximidamide (2)**: white solid. Yield = 85.6%. ^{1}H NMR (300 MHz, DMSO-d6) δ: 9.51 (s, 1H), 7.21 – 7.17 (m, 2H), 6.90 (d, J = 8.7 Hz, 1H), 6.03 (s, 2H), 5.73 (s, 2H).

2.4. Synthesis of 1,2,4-Oxadiazole (3)

N-Hydroxy-1,3-benzodioxole-5-carboximidamide (4.7 g; 26.1 mmol) was dissolved in toluene, and pentadecafluorooctanoyl chloride (13 mL; 2 mol eq.) together with pyridine (4.2 mL; 2 mol eq.) were added. The reaction mixture was refluxed for 6 h. After evaporation to dryness, water was added while maintaining the pH between 4 and 5. The product was isolated by extraction with ethyl acetate and purified by column chromatography, using a 10:1 petroleum ether/ethyl acetate mixture as the eluent. A white solid was obtained. **Compound (3)**: white solid. Yield = 45.5%. ^{1}H NMR (300 MHz, $CDCl_3$) δ: 7.70 (dd, J = 8.1, 1.4 Hz, 1H), 7.55 (s, 1H), 6.93 (d, J = 8.1 Hz, 1H), 6.07 (s, 2H).

2.5. Synthesis of the Perfluoroalkylated Triazole Derivative (4)

Compound (3) (0.5 g; 0.89 mmol) was dissolved in 3 mL of *N,N*-dimethylformamide, and methylhydrazine (471 µL; 10 mol eq.) was added. The reaction was carried out at 153 °C for 2 h, leading to the formation of a perfluoroalkylated triazole ring. The reaction mixtures were combined in a flask, water was added, and the solution was neutralized with HCl. The product was isolated by extraction with diethyl ether and purified by column chromatography, using a 5:1 petroleum ether/ethyl acetate mixture as the eluent. A white solid was obtained. **Compound (4)**: white solid. Yield = 76%. ^{1}H NMR (300 MHz, $CDCl_3$) δ: 7.21 – 7.18 (m, 2H), 6.95 (d, J = 7.8 Hz, 1H), 6.07 (s, 2H), 4.06 (s, 3H).

2.6. Synthesis of the Compound (5)

Compound (4) (0.5 g; 0.87 mmol) was dissolved in toluene (50 mL) and reacted with BBr_3 (250 µL; 3 mol eq.) under reflux for 3 h. Water was then added, and the reaction was maintained under reflux for an additional 30 min. The reaction mixture was transferred to a flask, concentrated to dryness to remove toluene, then water was added and the mixture was neutralized with a saturated $NaHCO_3$ solution. The product was isolated by extraction with ethyl acetate and purified by column chromatography, using a 5:1 petroleum ether/ethyl acetate mixture as the eluent. A yellow liquid was obtained. **Compound (5)**: Yellow liquid. Yield = 80%. ^{1}H NMR (300 MHz, $CDCl_3$) δ: 7.12 (s, 1H), 6.96 (d, J = 8.2 Hz, 1H), 6.88 (d, J = 8.2 Hz, 1H), 4.01 (s, 3H).

2.7. Synthesis of the Triazole precursor (6)

In a pressure tube, compound (5) (0.4 g; 0.715 mmol) was dissolved in acetonitrile (7 mL), followed by the addition of K_2CO_3 (0.6 g; 6 mol eq.). Subsequently, 1-bromotetradecane (1 mL; 5 mol eq.) was added. The reactions were maintained at 82 °C under stirring. The formation of the perfluoroalkyl-substituted triazoles was monitored by Thin-Layer Chromatography. The reaction mixture was transferred into a 250 mL flask, concentrated to dryness to remove acetonitrile, then water was added and the mixture was neutralized by addition of HCl. The product was isolated and purified by extraction with ethyl acetate followed by column chromatography, using a 20:1 petroleum ether/ethyl acetate mixture as the eluent. The product was obtained as white solid. **Compound (6)**: white solid. Yield = 82%. ^{1}H NMR (300 MHz, $CDCl_3$) δ: 7.24 (d, J = 9.6 Hz, 1H), 7.19 (dd, J = 8.3, 1.8 Hz, 1H), 6.97 (d, J = 8.3 Hz, 1H), 4.10

– 4.02 (m, 7H), 1.84 (h, J = 6.3 Hz, 4H), 1.55 – 1.21 (m, 44H), 0.87 (t, J = 6.3 Hz, 6H).

2.8. Synthesis of Trifluoromethanesulfonate Triazolium Salt

A solution of Compound (6) (0.5 g; 0.52 mmol) in toluene (10 mL) was placed in a sealed tube, and $CF_3SO_2OCH_3$ (1.5 mL; 26 mol eq.) was added. The mixture was heated at 110 °C for 2 h. After completion, the reaction was concentrated under reduced pressure to remove toluene, followed by addition of water and neutralization of the excess $CF_3SO_2OCH_3$ with NaOH. The product was isolated by extraction with ethyl acetate and purified by column chromatography using a 5:1 petroleum ether/ethyl acetate mixture as the eluent. The compound was obtained as a white solid. HPLC-MS analysis confirmed the identity of the compound and the absence of significant organic impurities. **5-(3,4-bis(tetradecyloxy) phenyl)-1,4-dimethyl-3-(perfluoroheptyl)-1H-1,2,4-triazol-4-ium trifluoromethanesulfonate [Tr-7,p-m14][OTf] (7)**: white solid. Yield = 67%. ^{1}H NMR (300 MHz, $CDCl_3$) δ: 7.45 (d, J = 2.1 Hz, 1H, Har), 7.24 (d, J = 2.0 Hz, 1H, Har), 7.08 (d, J = 8.5 Hz, 1H, Har), 4.13 – 4.04 (m, 7H, OCH_2 + N-CH_3), 3.90 (s, 3H, N-CH_3), 1.85 (dt, J = 14.2, 7.2 Hz, 4H, CH_2), 1.48 (q, J = 7.2 Hz, 4H, CH_2), 1.26 (d, J = 2.4 Hz, 40H, CH_2), 0.90 – 0.84 (m, 6H, CH_3). HRMS: m/z = calcd for $C_{45}H_{67}F_{15}N_3O_2$ $[M]^+$ 966.4988; found 966.5008. The triflate triazolium salt obtained in Section 2.8 is reported here and its preparation is described above. Two other triazolium triflate salts used as precursors for the anion-exchange (metathesis) reactions were synthetized according to previously published procedures [11,21] and are therefore not detailed here.

2.9. Synthesis of Bis(trifluoromethanesulfonyl)imide Salts

In separate 50 mL flasks, methyl triflate salts (80 mg; 0.08 mmol) were dissolved in methanol (5 mL). Lithium bis (trifluoromethanesulfonyl)amide (3.5 mol eq.) was added, and the mixtures were stirred at 40 °C for approximately 15 min. Water was then added dropwise until complete precipitation of the bis (trifluoromethanesulfonyl)imide salts occurred. The products were obtained as white solids. HPLC-MS analysis confirmed the identity of the compound and the absence of significant organic impurities. **5-(3,4-bis(tetradecyloxy)phenyl)-1,4-dimethyl-3-(perfluoroheptyl)-1H-1,2,4-triazol-4-ium trifluoromethanesulfonate [Tr-7,p-m14][NTf_2] (8)**: white solid. Yield = 91%. ^{1}H NMR (300 MHz, Acetone-d6) δ: 7.51 (dd, J= 8.7, 1.6 Hz, 1H, Har), 7.45 (d, J = 1.4 Hz, 1H, Har), 7.38 (d, J = 8.4 Hz, 1H, Har), 4.30 (s, 3H, N-CH_3), 4.24 – 4.14 (m, 5H, OCH_2 + N-CH_3), 4.09 (t, J= 6.2 Hz, 2H, OCH_2), 1.95 –1.75 (m, 4H, CH_2), 1.63 –1.20 (m, 44H, CH_2), 0.88 (t, J= 5.8 Hz, 6H, CH_3). HRMS: m/z = calcd for $C_{45}H_{67}F_{15}N_3O_2$ $[M]^+$ 966.4988; found 966.5004. **5-(3,5-bis (tetradecyloxy)phenyl)-1,4-dimethyl-3-(perfluoroheptyl)-1H-1,2,4-triazol-4-ium trifluoromethanesulfonate [Tr-7,m-m14] [NTf_2] (9)**: white solid. Yield = 80%. ^{1}H NMR (300 MHz, CDCl3) δ: 6.80 (s, 3H, Har), 4.12 (s, 3H, N-CH_3), 4.07 (t, J = 8.3 Hz, 2H, OCH_2), 4.00 (t, J = 5.5 Hz, 2H, OCH_2), 3.93 (s, 3H, N-CH_3), 1.86 – 1.73 (m, 4H, CH_2), 1.51 – 1.21 (m, 44H, CH_2), 0.87 (t, J = 6.6 Hz, 6H, CH_3). HRMS: m/z = calcd for $C_{45}H_{67}F_{15}N_3O_2$ $[M]^+$ 966.4988; found 966.4994.

2.10. Synthesis of Hexafluorophosphate Salts

In separate 50 mL flasks, methyl triflate salts (80 mg; 0.08 mmol) were dissolved in methanol (5 mL). Ammonium hexafluorophosphate (3.5 mol eq.) was added, and the mixtures were stirred at 40 °C for approximately 15 min. Water was then added dropwise until complete precipitation of the hexafluorophosphate salts occurred. The products were obtained as white solids. HPLC-MS analysis confirmed the identity of the compound and the absence of significant organic impurities. **5-(4-(tetradecyloxy)phenyl)-1,4-dimethyl-3-(perfluoroheptyl)-1H-1,2,4-triazol-4-ium trifluoromethanesulfonate [Tr-7,p14][PF_6] (10)**: white solid. Yield = 63%. ^{1}H NMR (300 MHz, Acetone-d6) δ: 7.90 (d, J = 8.8 Hz, 2H, Har), 7.37 (d, J = 8.8 Hz, 2H, Har), 4.28 (s, 3H, N-CH_3), 4.20 (t, J = 6.5 Hz, 2H, OCH_2), 4.15 (s, 3H, N-CH_3), 1.92 – 1.78 (m, 2H, CH_2), 1.57 – 1.24 (m, 22H, CH_2), 0.87 (t, J = 6.4 Hz, 3H, CH_3).
HRMS: m/z = calcd for $C_{31}H_{39}F_{15}N_3O$ $[M]^+$ 754.2848; found 754.2854. **5-(3,4-bis(tetradecyloxy)phenyl)-1,4-dimethyl-3-(perfluoroheptyl)-1H-1,2,4-triazol-4-ium trifluoromethanesulfonate [Tr-7,p-m14][PF_6] [11]**: white solid. Yield = 89%. 1H NMR (300 MHz, CD3CN) δ: 7.23 (s, 2H, Har), 7.10 (s, 1H, Har), 4.12 (t, J = 6.3 Hz, 2H, OCH_2), 4.04 (t, J = 6.2 Hz, 2H, OCH_2), 4.00 (s, 3H, N-CH_3), 3.81 (s, 3H, N-CH_3), 1.89 – 1.73 (m, 4H, CH_2), 1.59 – 1.20 (m, 44H, CH_2), 0.88 (t, J = 6.4 Hz, 6H, CH_3). HRMS: m/z = calcd for $C_{45}H_{67}F_{15}N_3O_2$ $[M]^+$ 966.4988; found 966.5011. **5-(3,5-bis(tetradecyloxy)phenyl)-1,4-dimethyl-3-(perfluoroheptyl)-1H-1,2,4-triazol-4-ium trifluoromethanesulfonate [Tr-7,m-m14][PF_6] (12)**: white solid. Yield = 51%. ^{1}H NMR (300 MHz, CD3CN δ: 6.87 (t, J = 1.8 Hz, 1H, Har), 6.72 (d, J = 1.9 Hz, 2H, Har), 4.04 (t, J = 6.6 Hz, 4H, OCH_2), 4.01 (s, 3H, N-CH_3), 3.81 (s, 3H, N-CH_3), 1.84 – 1.70 (m, 4H, OCH_2), 1.52 – 1.23 (m, 44H, CH_2), 0.88 (t, J = 6.4 Hz, 6H, CH_3). HRMS: m/z = calcd for $C_{45}H_{67}F_{15}N_3O_2$ $[M]^+$ 966.4988; found 966.4996.

3. Results and Discussion

3.1. Synthesis of ILCs

ILCs were prepared following the multistep sequence shown in **Scheme 2**. Starting from piperonal, the amidoxime precursor (2) was obtained and converted into the corresponding 1,2,4-oxadiazole (3) by reaction with the selected perfluoroacyl chloride. Treatment of this oxadiazole with methylhydrazine induced an ANRORC-type transformation leading to formation of the 1,2,4-triazole scaffold (4). The reaction of triazole (4) with BBr_3 cleaved the methylenedioxy (acetal) unit to give the corresponding di-hydroxy intermediate (5). This intermediate (5) was alkylated with tetradecyl halide to deliver the dialkyloxy-phenyl 1,2,4-triazoles [Tr -7,p-m14] (6). Final *N*-methylation with methyl trifluoromethanesulfonate produced the corresponding triazolium triflate salt [Tr-7,p-m14][OTf] (7). Consistent with prior reports, methylation of these 3,4-disubstituted 1,2,4-triazoles proceeds

preferentially at the less sterically hindered and more nucleophilic N(4) site [11]. As noted above, two triazolium triflates used in this study were prepared following previously published procedures [11,21]. A third triazolium triflate was synthesized according to the workflow described in Section 2.8. All the three triflate salts were then employed as precursors in the anion-exchange protocol described here. As shown in **Scheme 3**, the three triazolium triflates were converted, by metathesis, into five distinct triazolium salts through replacement of OTf^- with either NTf_2- or PF_6^-. The products of these transformations are two NTf_2^- salts, [Tr-7,p-m14][NTf_2] (8) and [Tr-7,m-m14][NTf2] (9), and three PF_6 salts, [Tr-7,p14][PF_6] (10), [Tr-7,p-m14][PF_6] (11) and [Tr-7,m-m14][PF_6] (12) (see **Scheme 3** for the general reaction representation). By converting a common triazolium triflate platform into salts with markedly different counter-ions, the metatheses provide a controlled approach to probe how anion nature (NTf_2^- vs PF_6^- vs OTf^-) modulates mesomorphic windows, thermal transitions and ionic interactions in this class of perfluoroalkyl triazolium ILCs. The DSC and POM data discussed below directly compare the metathesis products with the parent triflate salts in order to isolate the role of the counter-anion in determining phase type, transition temperatures and textural features.

3.2. Thermal and *POM* analysis

The thermal behavior of all compounds was examined by DSC and POM. An initial rapid heating scan was carried out to ensure reproducible thermal conditions. Data reported correspond to the first cooling and the second heating scans and were reproducible upon further cycling (see **Figure SM1**, Supporting Information). Transition temperatures, transition enthalpies and the phase changes observed for the six ILCs studied are listed in **Table 1**.

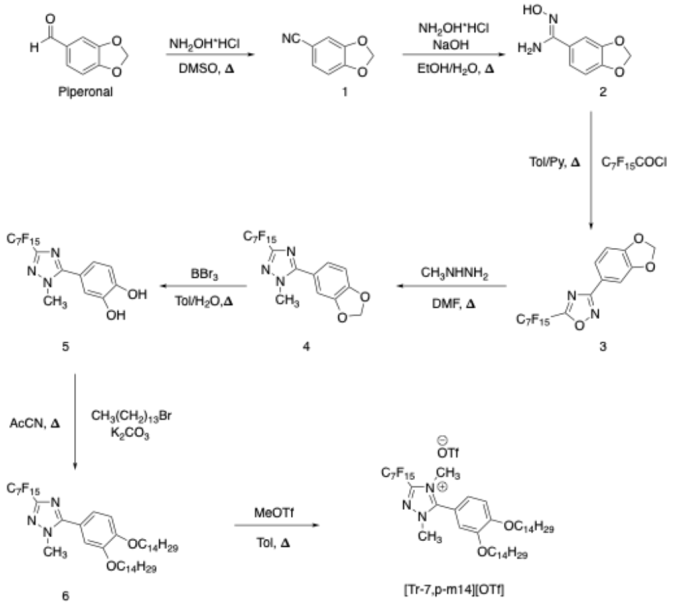

Scheme 2 | Synthetic route to triazole precursor 6 and to the related OTf^- salt.

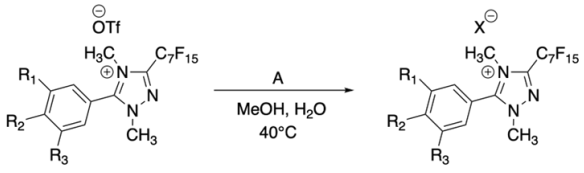

Name Compound	R_1	R_2	R_3	X
[Tr-7,p-m14][NTf_2]	-$OC_{14}H_{29}$	-$OC_{14}H_{29}$	-H	NTf_2
[Tr-7,m-m14][NTf_2]	-$OC_{14}H_{29}$	-H	-$OC_{14}H_{29}$	NTf_2
[Tr-7,p14][PF_6]	-H	-$OC_{14}H_{29}$	-H	PF_6
[Tr-7,p-m14][PF_6]	-$OC_{14}H_{29}$	-$OC_{14}H_{29}$	-H	PF_6
[Tr-7,m-m14][PF_6]	-$OC_{14}H_{29}$	-H	-$OC_{14}H_{29}$	PF_6

Scheme 3 | Synthetic route to Trifluoromethanesulfonate Triazolium Salt.

Table 1 | Melting temperatures (T_m) and clearing temperatures (T_c) along with the corresponding enthalpies (ΔH) of triazolium salts obtained from the DSC traces upon heating and cooling.

Compound	Heating Cycles			Cooling Cycles		
	T_m (°C)[a]	ΔH (KJ mol^{-1})	Transition[c]	T_c (°C)[b]	ΔH (KJ mol^{-1})	Transition[c]
[Tr-7,p14][PF_6] (10)	74.2	45.3	*Cr → LC			
	165.7	4.5	LC→ LC'	193.7	4.3	Iso → LC'
	196.7	4.2	LC' → Iso	158.7	3.4	LC' → LC
[Tr-7,p-m14][OTf] (7)				146.9	5.53	Iso → LC"
	77.9	19.5	Cr → LC	116.3	0.6	LC" → LC'
	117.8	0.8	LC → LC'	80.4	6.1	LC' → LC
	146.5	5.6	LC' → Iso	67.2	7.1	LC → Cr
[Tr-7,p-m14][NTf_2] (8)	46.7	35.2	Cr → LC	112.2	2.0	Iso → LC'
	80.2	3.9	LC → LC'	70.8	3.4	LC' → LC
	115.7	3.5	LC' → Iso	41.2	34.2	LC → Cr
[Tr-7,p-m14][PF_6] (11)	22.7	13.7	Cr → LC	176.4	3.4	Iso → LC'
	171.6	12.2	LC → Iso	167.5	3.7	LC' → LC
				25.1	15.6	LC → Cr
[Tr-7,m-m14][NTf_2] (9)	-8.3	6.5	Cr → Cr'	67.3	2.9	Iso → LC
	11.6	4.2	Cr' → Cr"	32.5	6.6	LC → Cr"
	33.9	3.6	Cr" → LC	7.2	4.3	Cr" → Cr'
	54.7	16.5	LC → Iso	-7.7	4.6	Cr' → Cr
[Tr-7,m-m14][PF_6] (12)	6.7	-	Cr → G	138.2	2.9	Iso → LC
	132.7	20.6	G → LC	126.7	8.5	LC → G
	141.2	**	LC → Iso	3.1	-	G → Cr

[a] Transitions refer to the second heating cycles. Temperatures indicate the onset of each peak.

[b] Transitions refer to the first cooling cycles. Temperatures indicate the onset of each peak.

[c] Abbreviations: Iso - isotropic phase; LC - liquid crystalline phase; G - glass transition and Cr - crystalline solid state.

*Transition observed only after the first heating cycle and not detected in subsequent cycles.

** ΔH value is not reported due to broadening and overlapping DSC signals.

In all cases more than one transition can be observed from DSC traces both during heating and cooling ramps (**Figures 1 and 2**). For 4-substituted salt [Tr-7,p14][PF_6] (10), three transitions are detected during the first heating, though one of these events disappears from all subsequent heating cycles. From the second heating onward, the thermogram displays only two reproducible mesophase transitions, LC → LC' and LC' → Iso, indicating that the system adopts a stable mesomorphic sequence after the initial thermal activation. Upon cooling the material undergoes the Iso → LC' transition at the clearing temperature, followed by an internal reorganization within the mesophase (LC' → LC) (**Figure 1**), without reaching a crystalline ordered phase in the range of scanned temperature. The disappearance of the Cr → LC event after the first heating, combined with the fully reproducible mesophase behavior observed thereafter, is consistent with an irreversible rearrangement of the initial solid-state packing during the first thermal excursion. Similar transitions detectable exclusively in the initial heating cycle have been reported for both low molecular weight liquid crystals and ionic mesogens, where metastable crystalline domains convert into a more stable organization upon heating, eliminating the corresponding transition in subsequent scans [22,23]. [Tr-7,p-m14][OTf] (7) produced a multi-step thermotropic behavior. On heating, the OTf^- salt undergoes a Cr → LC transition, followed by a LC → LC' reorganization and a final LC' → Iso clearing. The relatively large enthalpy of the low-temperature Cr → LC step indicates substantial loss of crystalline order upon entry into the first mesophase, whereas the small enthalpy for the LC → LC' step is typical of intramesophase rearrangements involving changes in lateral packing without gross positional disordering. During cooling the isotropic melt first forms a higher-temperature mesophase (Iso → LC''), which subsequently transforms to the lower-temperature mesophases sequence (LC'' → LC', LC' → LC) before finally crystallizing (LC → Cr). The cooling data show that the system accesses a succession of ordered states on cooling that mirror, in reverse, the heating reorganizations. The differences in onset temperatures and enthalpies indicate modest hysteresis and suggest that the LC↔LC' conversions are reversible but kinetically hindered to some extent. Overall, the OTf^- salt displays clear multistep mesomorphic behavior in both scan directions, consistent with competing packing motifs stabilized by the relatively small coordinating OTf^- anion [1,24] (**Figure 2**). The NTf_2^- analogue showed three transitions on heating, which can be attributed to Cr → LC, LC → LC', and LC' → Iso. The very large enthalpy associated with the low-temperature crystalline loss suggests entry into a well-ordered mesophase with substantial disruption of the original crystalline lattice. On cooling the reverse sequence is observed: Iso → LC', LC' → LC and LC → Cr. The comparable magnitude of the crystallization enthalpy on cooling and the melting-like enthalpy on heating supports the assignment of a well-defined LC phase that forms and disappears with significant latent heat. The NTf_2^- anion, being bulky and highly delocalized, often reduces ion pairing and enhances fluidity, which can stabilize distinct mesophases separated by modest LC ↔ LC' enthalpies [1,25]. This behavior is consistent with the clear, well-separated transitions observed here. The modest hysteresis between heating and cooling for the LC ↔ LC' steps suggests that these reorganizations are near-thermodynamic in nature but still subject to finite nucleation barriers (**Figure 2**) [26]. For [Tr-7,p-m14][PF_6] (11) the heating trace shows a low-temperature Cr → LC event and a single higher-temperature LC → Iso clearing, indicating a large mesomorphic stability window on heating. The cooling cycle, however, reveals a more complex path going from Iso → LC', LC' → LC to LC → Cr.

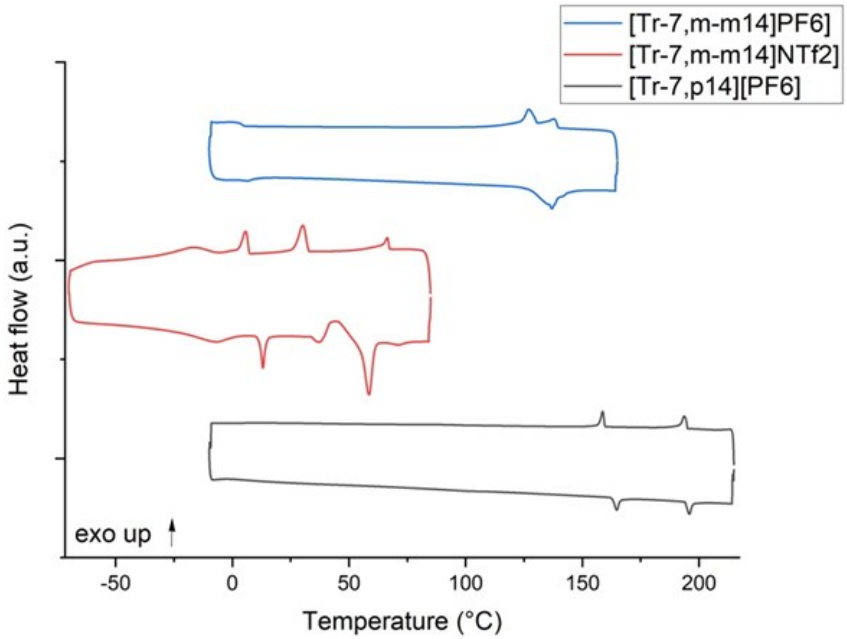

Figure 1 | DSC traces of PF_6^- and NTf_2^- triazolium salts. DSC traces of the 4- and 3,5-substituted PF_6^- and NTf_2^- triazolium salts, showing the main crystalline-mesophase transitions observed on heating and cooling.

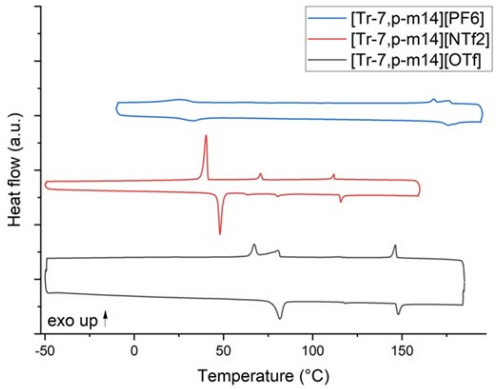

Figure 2 | DSC traces of OTf^-, NTf_2^- and PF_6^- triazolium salts. DSC traces of the p-m substituted OTf^-, PF_6^- and NTf_2^- triazolium salts, highlighting the multi-step mesophase behaviors and the counter-ion–dependent transition profiles.

The difference between the heating trace and the cooling one either suggests that certain mesophase reorganizations are kinetically accessible primarily upon cooling or small enthalpy LC ↔ LC' events may be masked by broadened baselines on heating. The PF_6^- anion, being more compact and less polarizable than NTf_2^-, probably tends to favor tighter ionic lattices and may restrict the mobility needed for some mesophase transformations during heating, hence producing the observed difference (**Figure 2**). [Tr-7,m-m14][NTf_2] (9) presents a sequence of low-temperature solid–solid transitions on heating (Cr → Cr', Cr' → Cr''), followed by Cr → LC and LC → Iso. The cooling run reproduces the mesophase formation (Iso → LC), followed by LC → Cr'', Cr'' → Cr and Cr' → Cr. The comparatively low temperatures and moderate enthalpies of the Cr → LC and LC → Iso steps indicate modest mesophase stability, consistent with m–m substitution producing less favorable mesomorphic packing than 4-substituted isomers (**Figure 1**). [Tr-7,m-m14][PF_6] (12) shows a low-temperature glass transition, followed on heating by Cr' → LC and LC → Iso. On cooling, the system passes from Iso → LC to LC → Cr' and finally Cr' → Cr. The presence of a glass transition suggests that at low temperatures the system falls out of equilibrium and that recrystallization might be kinetically limited. However, the formation of a mesophase with substantial enthalpy (Cr' → LC) indicates robust mesomorphic ordering at elevated temperatures. The high-temperature mesophase window and the relative magnitudes of ΔH on heating and cooling align with PF_6^- favoring well-defined but possibly less fluid mesophases compared with NTf_2^- analogues (**Figure 1**). A comparison of the transition temperatures of the newly synthesized compounds with those of the corresponding analogues previously reported in the literature [11,21] confirms the strong influence of the counter-ion on the mesophase behaviors. Moving from the smallest anion PF_6^- to the larger one NTf_2^- resulted in a decrease of both melting and clearing temperatures. The stability range of the mesophases also depends on the cation structure. Cations bearing alkyl substituents in the 3,5-positions, which provide a more extended and symmetric shape, displayed narrow mesophase windows, ranging from about 4 °C for the OTf^- salt to about 14 °C for the NTf_2^- salt. By contrast, cations with a single long alkyl chain in the 4-position, or with alkyl chains in the 3,4-positions, present considerably wider mesophase ranges and a larger number of distinct mesophases (**Figure 3**). Phase identification by POM was carried out during heating and cooling ramps and the textures of

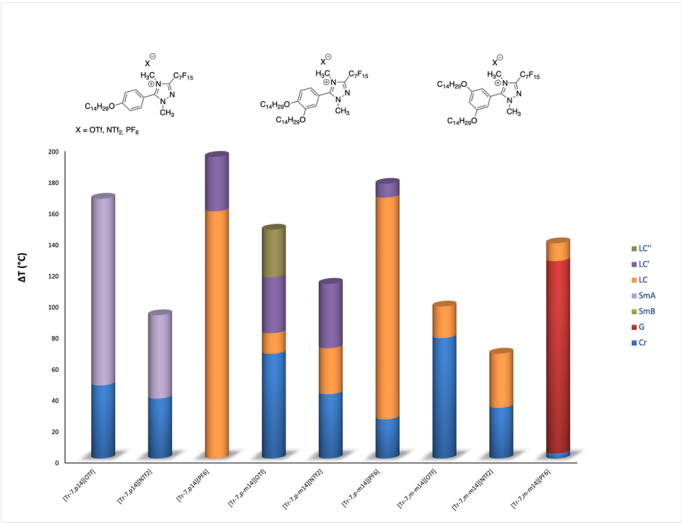

Figure 3 | Comparative DSC traces and POM analysis with literature analogues. DSC analysis of the triazolium salts studied in this work together with the previously reported analogues [11,21], recorded during the cooling ramp. The traces highlight the characteristic thermal transitions and phase-change behavior across the different substitution patterns and counter-ion.

the mesophases were examined to understand the liquid-crystalline nature. Materials that showed focal-conic textures under crossed polarizers were identified as smectic mesophases [26,27] (**Figure 4**), while marble-like textures, characteristic of layered ordering, were observed for compounds bearing two long alkyl chains (**Figure 5**). By the POM analysis, single-chain (4-substituted) derivatives showed focal-conic textures, ascribable to smectic phases. In particular, a SmA-like on cooling from the isotropic liquid was observed in [Tr-7,p-14][PF_6] (10), and a further transition (SmA ↔ SmB) at lower temperature (105 °C). This interpretation is consistent with previous reports on triazolium and other ionic liquid crystals [2,21]. On the other hand, it is noteworthy that [Tr-7,p-m14][PF_6] (11), [Tr-7,p-m14][OTf] (7) and [Tr-7,m-m14][PF_6] (12) exhibited dendritic growth on cooling from the isotropic liquid, a behavior commonly associated with discotic mesophases and consistent with supramolecular aggregation of the mesogens into disk-like assemblies.

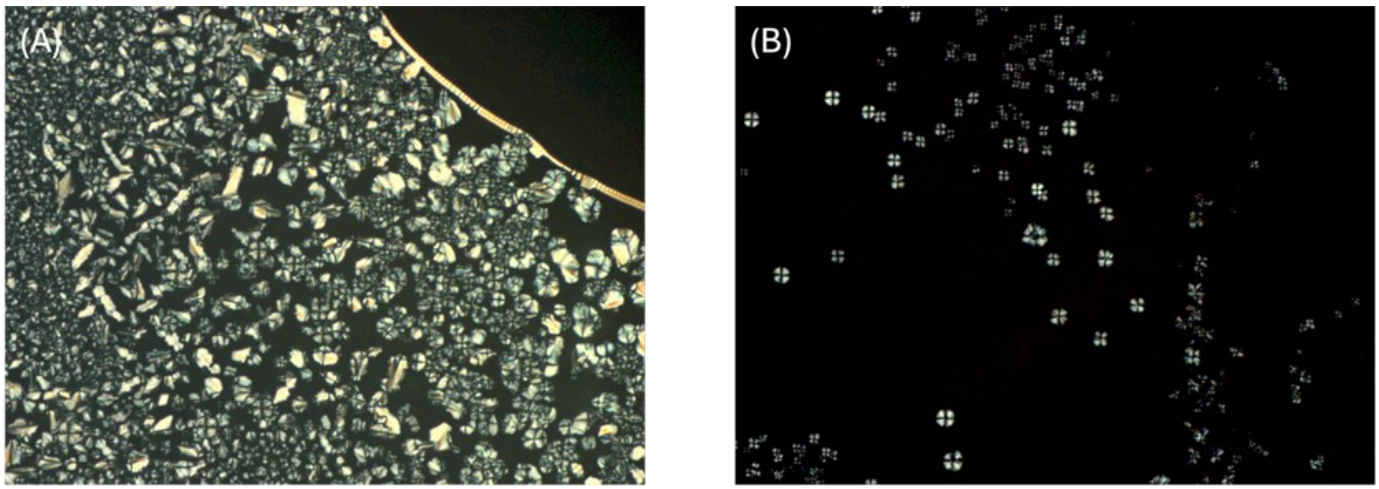

Figure 4 | Focal-conic textures. Microphotographs of selected focal conic textures observed in the studied materials, obtained upon cooling from the isotropic liquid. (A) SmB mesophase of [Tr-7,p14][PF_6] (10) recorded at 105 °C (200x). (B) SmA mesophase of [Tr-7,p14][PF_6] (10) recorded at 197 °C (200x).

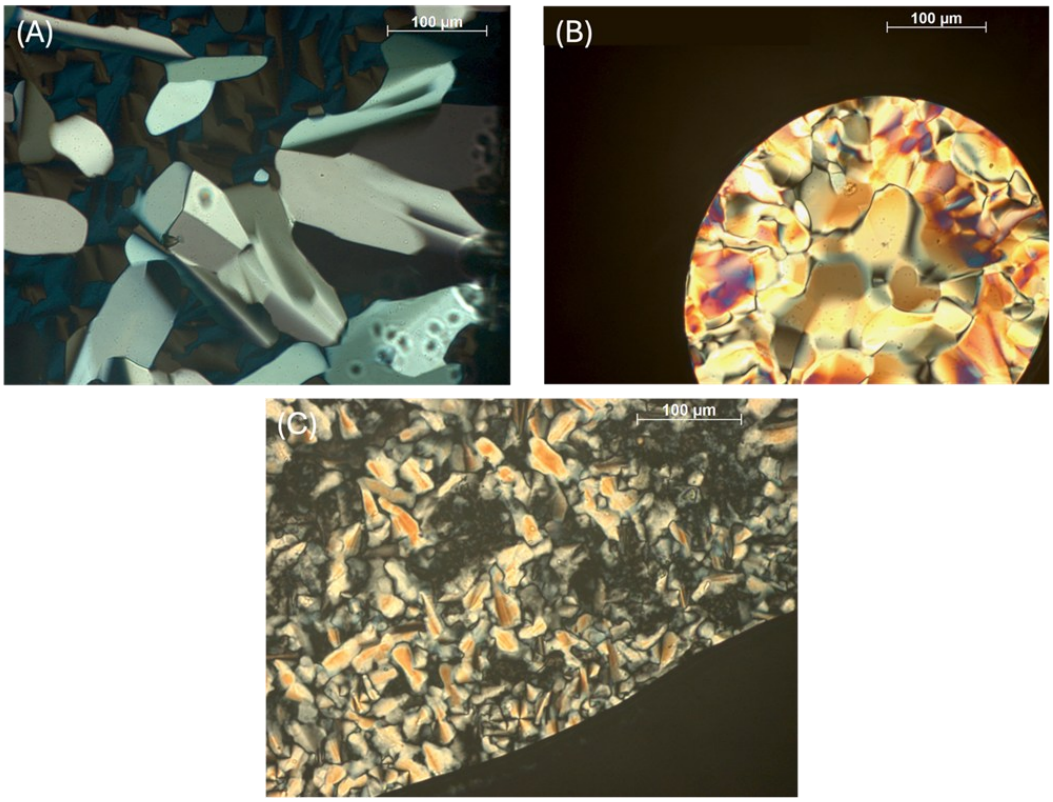

Figure 5 | Marble-like textures. Microphotographs of selected marble-like textures observed in the studied materials, obtained upon cooling from the isotropic liquid. (A) LC mesophase of [Tr-7,p-m14][OTf] (7) recorded at 149 °C (100x). (B) LC mesophase of [Tr-7,p-m14][PF_6] (11) recorded at 172.7 °C (100x). (C) LC' mesophase of [Tr-7,m-m14][PF_6] (12) recorded at 138 °C (200x).

Concluding Remarks

Six ILCs derived from 3-perfluoroalkyl-1,2,4-triazolium cores were synthesized and characterized to assess how thermal behavior is affected by counter-ion and by the alkyl substitution pattern on the phenyl ring. DSC results showed a systematic trend: for the series studied, NTf_2^- derivatives generally present lower melting and clearing temperatures than their corresponding PF_6^- analogues. Mesophase stability and the number of observed mesophases are cation dependent and strongly influenced by the alkyl substitution pattern on the phenyl ring. Cations bearing two alkyl chains in the 3,5-positions display relatively narrow mesophase windows, whereas cations with a single long chain at the 4-position or with 3,4-substitution exhibit broader mesophase ranges and a larger number of distinct transitions. POM observations can give information about LC transition nature: single-chain (4-substituted) derivatives show focal-conic textures consistent with smectic phases, while dialkyloxy derivatives give marble-type textures. Notably, dendritic growth on cooling from the isotropic liquid was observed in [Tr-7,p-m14][PF_6] (11), [Tr-7,p-m14][OTf] (7) and [Tr-7,m-m14][PF_6] (12), morphologies consistent with discotic-type supramolecular aggregation. These results indicate that the interplay between cation shape and anion volume determines not only the onset temperatures of mesophase formation but also the accessibility of intramesophase reorganizations (LC ⟷ LC', SmB ⟷ SmA). Broad, stable mesophase windows are favored by 4-substitution and by the NTf_2^- anion, whereas PF_6^- and more symmetric 3,5-substituted cations stabilize narrower, higher-temperature mesophase regimes. Enthalpy changes can further support these assignments, with larger ΔH values marking transitions between crystalline and mesomorphic states, and smaller ΔH values characterizing orientational rearrangements within the liquid-crystalline phases. Overall, these findings underscore that selective anion exchange combined with controlled cation substitution provides an effective strategy to tune mesophase type, thermal stability, mesophase breadth, and the richness of phase sequences in triazolium-based ionic liquid crystals. The structure-mesophase relationships identified here offer directly transferable criteria for designing fluorinated ionic liquid crystals as functional materials in anisotropic electrolytes, directional ion-transport systems for devices in which fine control of mesophase windows and supramolecular order is crucial.

Supplementary Material

The following supplementary material is available: **Table SM1**: LDSC analysis of the p-m substituted OTf^-, PF_6^- and NTf_2^- triazolium salts, highlighting the multistep mesophase behavior, the counterion-dependent transition profiles, and the reproducibility across multiple heating-cooling cycles.

Author contributions

Conceptualization, I.P.; Methodology, I.P., A.P.; Formal analysis, I.P. C.R. and I.F.; Investigation, I.F., D.R., C.R.; Writing—original draft, I.F., C.R.; Writing—review & editing, I.P., C.R., D.R.; Visualization, A.P., D.R.; Supervision, I.P.; Funding acquisition, I.P. All authors have read and agreed to the published version of the manuscript.

Acknowledgements

The University of Palermo is gratefully acknowledged.

References

[1] K.V. Axenov, S. Laschat, Thermotropic Ionic Liquid Crystals, Materials (Basel) 4 (2011) 206–259. https://doi.org/10.3390/ma4010206.

[2] K. Goossens, K. Lava, C.W. Bielawski, K. Binnemans, Ionic Liquid Crystals: Versatile Materials, Chem Rev 116 (2016) 4643–4807. https://doi.org/10.1021/cr400334b.

[3] N. Kapernaum, A. Lange, M. Ebert, M.A. Grunwald, C. Haege, S. Marino, A. Zens, A. Taubert, F. Giesselmann, S. Laschat, Current Topics in Ionic Liquid Crystals, Chempluschem 87 (2022) e202100397. https://doi.org/10.1002/cplu.202100397.

[4] A. Abate, A. Petrozza, G. Cavallo, G. Lanzani, F. Matteucci, D.W. Bruce, N. Houbenov, P. Metrangolo, G. Resnati, Anisotropic ionic conductivity in fluorinated ionic liquid crystals suitable for optoelectronic applications, J. Mater. Chem. A 1 (2013) 6572–6578. https://doi.org/10.1039/C3TA10990A.

[5] M. Hird, Fluorinated liquid crystals--properties and applications, Chem Soc Rev 36 (2007) 2070–2095. https://doi.org/10.1039/b610738a.

[6] Q. Ruan, M. Yao, D. Yuan, H. Dong, J. Liu, X. Yuan, W. Fang, G. Zhao, H. Zhang, Ionic liquid crystal electrolytes: Fundamental, applications and prospects, Nano Energy 106 (2023) 108087. https://doi.org/10.1016/j.nanoen.2022.108087.

[7] A.F.M. Santos, J.L. Figueirinhas, M. Dionísio, M.H. Godinho, L.C. Branco, Ionic Liquid Crystals as Chromogenic Materials, Materials 17 (2024) 4563. https://doi.org/10.3390/ma17184563.

[8] S . Buscemi, A. Pace, I. Pibiri, N. Vivona, D. Spinelli, Fluorinated heterocyclic compounds. An expedient route to 5-perfluoroalkyl-1,2,4-triazoles via an unusual hydrazinolysis of 5-perfluoroalkyl-1,2,4-oxadiazoles: first examples of an ANRORC-like reaction in 1,2,4-oxadiazole derivatives, J Org Chem 68 (2003) 605–608. https://doi.org/10.1021/jo0262762.

[9] F. Lo Celso, I. Pibiri, A. Triolo, R. Triolo, A. Pace, S. Buscemi, N. Vivona, Study on the thermotropic properties of highly fluorinated 1,2,4-oxadiazolylpyridinium salts and their perspective applications as ionic liquid crystals, Journal of Materials Chemistry 17 (2007) 1201–1208. https://doi.org/10.1039/b615190f.

[10] A. Riccobono, R.R. Parker, A.C. Whitwood, J.M. Slattery, D.W. Bruce, I. Pibiri, A. Pace, 1,2,4-Triazolium ions as flexible scaffolds for the construction of polyphilic ionic liquid crystals, Chemical Communications 54 (2018) 9965–9968. https://doi.org/10.1039/c8cc04704a.

[11] A. Riccobono, G. Lazzara, S.E. Rogers, I. Pibiri, A. Pace, J.M. Slattery, D.W. Bruce, Synthesis and mesomorphism of related series of triphilic ionic liquid crystals based on 1,2,4-triazolium cations, Journal of Molecular Liquids 321 (2021) 114758. https://doi.org/10.1016/j.molliq.2020.114758.

[12] M.S. Weber, M. Schulze, G. Lazzara, A.P. Piccionello, A. Pace, I. Pibiri, Oxadiazolyl-pyridinium as cationic scaffold for fluorinated ionic liquid crystals†, Applied Sciences (Switzerland) 11 (2021). https://doi.org/10.3390/app112110347.

[13] S. Buscemi, A. Pace, A.P. Piccionello, I. Pibiri, N. Vivona, G. Giorgi, A. Mazzanti, D. Spinelli, Five-to-six membered ring-rearrangements in the reaction of 5-perfluoroalkyl-1,2,4-oxadiazoles with hydrazine and methylhydrazine, Journal of Organic Chemistry 71 (2006) 8106–8113. https://doi.org/10.1021/jo061251e.

[14] I. Pibiri, A. Pace, S. Buscemi, N. Vivona, L. Malpezzi, Designing fluorous domains. synthesis of a series of pyridinium salts bearing a perfluoroalkylated azole moiety, Heterocycles 68 (2006) 307–321. https://doi.org/10.3987/COM-05-10633.

[15] I. Zama, G. Gorni, V. Borzatta, M.C. Cassani, C. Crupi, G. Di Marco, Fluorinated imidazolium salts having liquid crystal characteristics, Journal of Molecular Liquids 223 (2016) 749–753. https://doi.org/10.1016/j.molliq.2016.08.101.

[16] G. Cavallo, G. Terraneo, A. Monfredini, M. Saccone, A. Priimagi, T. Pilati, G. Resnati, P. Metrangolo, D.W. Bruce, Superfluorinated Ionic Liquid Crystals Based on Supramolecular, Halogen-Bonded Anions, Angew Chem Int Ed Engl 55 (2016) 6300–6304. https://doi.org/10.1002/anie.201601278.

[17] G. Cavallo, A. Abate, M. Rosati, G. Paolo Venuti, T. Pilati, G. Terraneo, G. Resnati, P. Metrangolo, Tuning of Ionic Liquid Crystal Properties by Combining Halogen Bonding and Fluorous Effect, Chempluschem 86 (2021) 469–474. https://doi.org/10.1002/cplu.202100046.

[18] A. Riccobono, A.C. Whitwood, R.R. Parker, S. Hart, A. Pace, J.M. Slattery, I. Pibiri, D.W. Bruce, Crystal and molecular structure of series of triphilic ionic liquid-crystalline materials based on the 1,2,4-triazolium cation, CrystEngComm 100 (2022). https://doi.org/10.1039/d2ce01354a.

[19] C. Tschierske, Liquid crystals: materials design and self-assembly, Springer Science & Business Media, 2012.

[20] G. Saielli, T. Margola, K. Satoh, Tuning Coulombic interactions to stabilize nematic and smectic ionic liquid crystal phases in mixtures of charged soft ellipsoids and spheres, Soft Matter 13 (2017) 5204–5213. https://doi.org/10.1039/c7sm00612h.

[21] C. Rizzo, I. Fiduccia, S. Buscemi, A. Palumbo Piccionello, A. Pace, I. Pibiri, Shaping 1,2,4-Triazolium Fluorinated Ionic Liquid Crystals, Applied Sciences (Switzerland) 13 (2023). https://doi.org/10.3390/app13052947.

[22] D.M. Duarte, R. Richert, K. Adrjanowicz, Watching the Polymorphic Transition from a Field-Induced to a Stable Crystal by Dielectric Techniques, Crystal Growth & Design 20 (2020) 5406–5412. https://doi.org/10.1021/acs.cgd.0c00626.

[23] W. Cao, Y. Wang, Phase Behaviors of Ionic Liquids Heating from Different Crystal Polymorphs toward the Same Smectic-A Ionic Liquid Crystal by Molecular Dynamics Simulation, Crystals 9 (2019) 26. https://doi.org/10.3390/cryst9010026.

[24] N.V. Ignat'ev, P. Barthen, A. Kucheryna, H. Willner, P. Sartori, A Convenient Synthesis of Triflate Anion Ionic Liquids and Their Properties, Molecules 17 (2012) 5319–5338. https://doi.org/10.3390/molecules17055319.

[25] F. Philippi, T. Welton, Targeted modifications in ionic liquids - from understanding to design, Phys Chem Chem Phys 23 (2021) 6993–7021. https://doi.org/10.1039/d1cp00216c.

[26] Peter J. Colling, M. Hird, Introduction to Liquid Crystals: Chemistry and Physics, 1st Edition, CRC Press, 1997. https://doi.org/10.1201/9781315272801.

[27] N. Osiecka-Drewniak, Z. Galewski, E. Juszyńska-Gałązka, Distinguishing the Focal-Conic Fan Texture of Smectic A from the Focal-Conic Fan Texture of Smectic B, Crystals 13 (2023) 1187. https://doi.org/10.3390/cryst13081187.